https://doi.org/10.5194/essd-2025-537
Preprint. Discussion started: 4 December 2025

Open Access Earth System Science Data Discussions

The OpenSat4Weather dataset: Ku-band satellite link data for precipitation monitoring

Roberto Nebuloni[1], Maximilian Graf[2], Greta Cazzaniga[3], François Mercier[4], and Maxime Turko[4]

[1]Institute of Electronics, Computer and Telecommunication Engineering (IEIIT) of the National Research Council of Italy (CNR)
[2]Department of Hydrometeorology, Deutscher Wetterdienst
[3]Laboratoire des Sciences du Climat et de l'Environnement, UMR 8212 CEA-CNRS-UVSQ, Université Paris-Saclay, IPSL, 91191 Gif-sur-Yvette, France
[4]Sereno / HD Rain, 198 avenue de France, Paris, France

Correspondence: Roberto Nebuloni (roberto.nebuloni@cnr.it)

Abstract. The TV-SAT signals received by the ground antennas of Satellite Microwave Links (SMLs) can be opportunistically used for identifying and quantifying precipitation. Hence, SMLs can serve as low-cost rainfall sensors complementary to conventional instruments. However, a significant challenge for opportunistic sensors, such as SMLs and their terrestrial counterpart, i.e., commercial microwave links (CMLs), stems from potential ownership issues, possibly hindering progress in the development of processing tools and validation studies. This underscores the critical need for open data. While CML open datasets are already available, there are no large SML datasets in public repositories. To fill this gap, we introduce here the OpenSat4Weather dataset, a comprehensive and openly accessible collection of data from 215 SML sensors located in Southern France, covering a five-month period from August to December 2022. The dataset is accessible at https://doi.org/10.5281/zenodo.16530166. OpenSat4Weather also includes concurrent conventional data: 6-minute rainfall depths from 113 operational rain gauges, and radar-based estimates of rainfall intensity along each SML path. The radar data are derived from the gauge-adjusted weather radar product Panthere from Météo-France. Additionally, ERA5 reanalysis data of the 0-degree isotherm height are provided for rain height estimation, which is essential for accurate conversion of the received signal level into rainfall intensity.

In this paper, we overview the OpenSat4Weather dataset. We detail the data preparation process and draw statistics of data availability. Furthermore, we present a descriptive analysis of the dataset, including an assessment of the observed rain characteristics, based on the rain gauges, and of the SML received power, and a comparison between SML and radar data. Finally, we provide examples of disturbances and anomalous patterns encountered on the SML raw data. Our ultimate goal is to promote open research that can help in accelerating the development of SML-based applications. Indeed, enhancing rainfall monitoring capabilities by opportunistic sensors could be beneficial in those areas where conventional networks are scarce.

https://doi.org/10.5194/essd-2025-537
Preprint. Discussion started: 4 December 2025

Open Access Earth System Science Data Discussions

1 Introduction

The effects of rainfall on Satellite Communications (SatCom) have been studied for several decades as signal fades due to rain significantly degrade the performance of satellite links operating in Ku band and above (Crane, 1996; ITU-R P.838-3, 2005). The large deployment of geostationary satellite fixed services such as TV-SAT or satellite internet in these rainfall sensitive bands paved the way for the opportunistic use of the signal received by a ground terminal to carry out rainfall measurements. The raw data collected by Satellite Microwave Links (SMLs) are the Received Signal Level (RSL), that is, either the power received by the ground terminal (usually expressed in units of dBm) or the signal-to-noise ratio (in dB), averaged over a suitable period of time. The time series of RSL go through a processing chain that identifies the rainy periods, separates the effects of rain from the ones of disturbances, and finally converts the cleaned up signal into rainfall intensity (Arslan et al., 2017).

Two different configurations have been proposed to implement the opportunistic sensing paradigm through SMLs. One is based on commercial-grade low-cost equipment including a satellite dish antenna, a receiver and a data logger storing TV-SAT broadcasting signals. The data collected in-situ by several of such devices are transferred to a central server for processing by a cellular or Wi-Fi connection, hence, setting-up a network of rainfall sensors with real-time capability (Colli et al., 2019; Gelbart et al., 2025). Flexibility is another key advantage of these sensors as they can be quickly deployed wherever is needed, for instance in regions where conventional sensors provide a poor coverage. A different scheme relies on satellite-based IoT services or Internet via satellite, which feature two-way links (Giannetti et al., 2019). In this case, the signal received by the user terminal at ground can be transmitted back to the gateway through the return channel. Data generated from many user terminals can be processed by a central server. Please note the difference between the two approaches. In the former case, an additional infrastructure has to be deployed and the raw data are available to anybody is willing to install a ground receiver. In the latter case, no additional infrastructure is necessary, as the RSL at ground is transmitted through the return channel (alongside user traffic) for operational purposes, for instance, to optimize link performance according to current channel conditions. However, in this case, the satellite operator is the owner of the data. Both SML schemes provide very high temporal resolution data, in the order of 1-min or even less.

The research on SMLs as opportunistic rainfall sensors has been inspired by similar studies on terrestrial backhauling links, namely Commercial Microwave Links (CMLs), which started nearly twenty years ago (Messer et al., 2006; Leijnse et al., 2007a). One advantage of CML data is ubiquitous coverage, as virtually any mobile network in the world features backhauling through wireless links. The relative density of wired (i.e. fiber) and wireless connections in a network depends on factors such as cost of the infrastructure and challenges posed by the environment. The exploitation scheme of CML data is similar to the one of two-way SMLs as in both cases data are generated as by-side products by the network operator for purposes of monitoring link performance. However, the processing chain of SML data has important differences with respect to CMLs. These peculiar aspects depend on the geometry of the link, which goes through the entire atmosphere, and on the characteristics of the transmitter, i.e., a geostationary satellite. In particular, only a small part of the link close to the ground and up the height where ice particles have melted into raindrops is affected by rain. Therefore, the knowledge of rain height is crucial to the correct conversion process from RSL to rainfall intensity as signal attenuation is proportional to the rainy propagation path

https://doi.org/10.5194/essd-2025-537
Preprint. Discussion started: 4 December 2025

(Giannetti et al., 2017). The rain height can be estimated by using measurements from weather radars or radiosoundings (when available), models, or, again, forecasts produced by NWPs. Moreover, significant errors in rainfall intensity estimates may be caused by the additional RSL loss due to the presence of the melting layer, that is, the thin part of the atmosphere above the rainy layer where melting particles are falling. Finally, the transmitted power level by the satellite is not known and not constant and the spacecraft undergoes movements produced by gravitational effects. All these factors induce unwanted RSL variations that overlap the ones due to rain. Despite the complexity of data processing, several studies demonstrated the performance of SMLs in detecting dry/wet periods (Angeloni et al., 2024; Gianoglio et al., 2024) as well as in quantifying precipitation (Barthès and Mallet, 2013; Mercier et al., 2015; Colli et al., 2020; Adirosi et al., 2021). The reference data used in the validation process are direct measurements from operational networks of rain gauges or from disdrometers, or, again, precipitation maps available as weather radars products.

It is very important to unlock CML and SML datasets, which may have ownership issues. Open data will help developing processing tools and carrying out validation studies, when concurrent datasets of conventional rainfall data are available. Research activity on open data can assess the quality of opportunistic rainfall data and whether they can be used in operational scenarios, paving the way for implementing new business models. A few open CML datasets are already available in the literature. For instance, the OpenMRG dataset includes raw data relative collected from 364 two-way links located in the urban area of Goteborg (Sweden) over a three-month summer period (Andersson et al., 2022). A countywide network of 1818 links covering the Netherlands, and spanning the period from January 2011 to March 2015 (with gaps) is illustrated in (Overeem et al., 2016). The above links are part of the network from one of the three mobile network operators active in the Netherlands. Finally, two years of data (2021 and 2022) collected from about 150 CMLs in the region of Emilia-Romagna (Italy) are available for open access on the Zenodo platform (Covi, E. and Roversi, G., 2024), as well as data from 100 links operated by the NYC Community Mesh network (Jacoby et al., 2025).

On the other hand, to the authors' knowledge, no widespread SML open datasets are accessible. This paper fills the gap, presenting OpenSat4Weather (Nebuloni et al., 2025), an open dataset that includes 215 SML sensors located in Southern France for a period of five months from August to December 2022 as well as concurrent conventional data collected by rain gauges and weather radars. Finally, meteorological data and a simple method for the evaluation of the rain height are provided.

2 Study area and data collection

The dataset covers the period from August to December 2022 and partially includes the coastal area near the Mediterranean Sea in southeastern France (Figure 1). The case study area is characterized by a Mediterranean climate, with mild winters, hot and dry summers, and wetter springs and autumns. Seasonal rainfall is often associated with thunder-storms, which contribute approximately 40% of the annual total and account for around 35% of rainy days (Table 1). This proportion is significantly higher compared to northern France. On the other hand, total precipitation accumulation is relatively low in the southeastern region compared to the southwestern region, with Biarritz being an extreme example (Table 1).

In the following subsections we describe the four different types of data that make up the OpenSat4Weather dataset.

https://doi.org/10.5194/essd-2025-537
Preprint. Discussion started: 4 December 2025

Open Access Earth System Science Data Discussions

Table 1. Average precipitation and average number of rainy days per year (1991–2020) for selected French cities (Météo-France).

City	Avg. annual precipitation (mm)	Rainy days >1 mm	Rainy days >10 mm	Proportion of >10 mm among >1 mm (%)
Biarritz	1473	141.1	49.9	35.4
Paris (Montsouris)	634.3	108.9	15.8	14.5
Montpellier (Airport)	639.2	57.8	17.7	30.6
Nîmes (Courbessac)	734.4	64.8	22.1	34.1
Marseille (Marignane)	532.3	53.5	15.8	29.5
Toulon	633.4	57.5	18.5	32.2
Nice	791.3	62.1	24.1	38.8

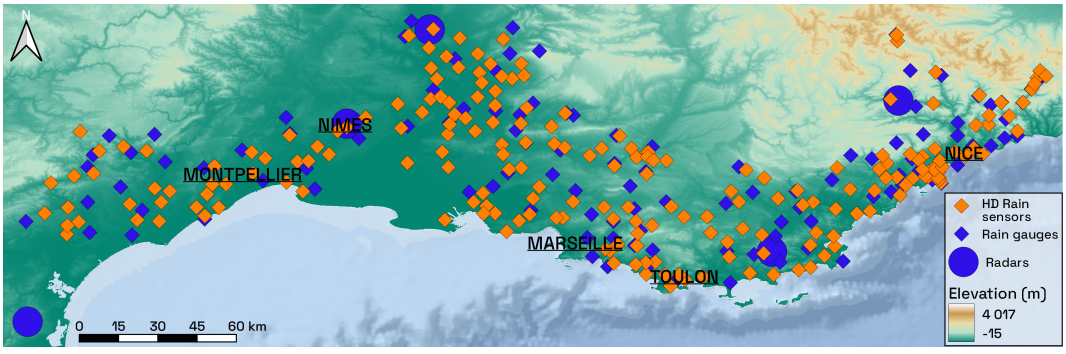

Figure 1. Position of the HD Rain SML stations, of rain gauges and radars in the coastal area near the Mediterranean Sea in southeastern France.

2.1 SML

SML data were courteously provided by HD Rain, a French company offering weather services. The deployment of HD Rain terminals in this region is driven by significant environmental and meteorological risks. The area is highly exposed to "épisodes cévenols", that is, intense Mediterranean rainfall events that can cause severe flash floods. Given the flood risk, high-resolution precipitation measurements are essential for improving early warning systems and hydrometeorological modelling, particularly in this region, which includes large densely urbanized areas where pluvial flooding poses major challenges. Additionally, the region's complex topography results in highly variable rainfall patterns, which makes conventional measurements difficult. SML terminals address this issue by providing low cost decentralised fine-scale precipitation data, enhancing meteorological observations in mountainous areas.

Beyond monitoring precipitation, integrating temperature and humidity sensors into these devices (Figure 2) also enables them to contribute to forest fire risk management in this region, which is particularly prone to such hazards.

By tackling these critical challenges, HD Rain terminals enhance both flood and wildfire risk management in the region.

https://doi.org/10.5194/essd-2025-537
Preprint. Discussion started: 4 December 2025

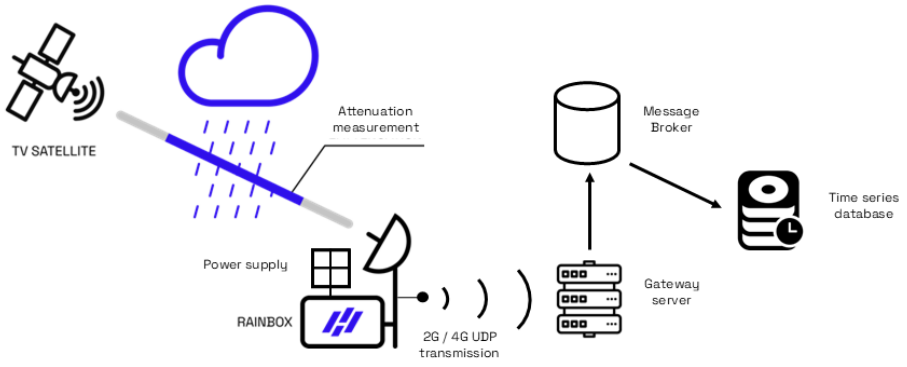

Figure 2. Sketch of SML configuration: HD Rain station and data transfer.

The SML sensor measures the loss of signal power, namely rain attenuation, caused by rainfall on the microwave signal transmitted by a broadcasting satellite (Figure 2). The average rain intensity between the receiving ground station and the rain-snow limit is proportional to rain attenuation. At the studied frequencies (Ku-band), dry snow is entirely transparent to the signal. Consequently, the rain-snow limit is often set at the 0°C isotherm, although the transition between snow and rain is more gradual due to the presence of the melting layer. Each HD Rain SML consists of a satellite dish (around 75 cm of diameter) with a standard TV Low-Noise Block (LNB), a solar panel, ensuring the station's autonomy, a GSM antenna, and a device called *Rainbox*. The latter includes a data logger that enables high-frequency measurement of the signal strength received from the satellite, resamples these measurements by averaging them over 15-second intervals, and contains a SIM card that ensures connectivity with various operators worldwide. These raw data are transmitted via the GSM network to a central server, where a message broker processes and decodes them, making the information usable and storable in a time-series database.

Table 2. Satellite characteristics and associated stations.

Satellite	**Owner**	**Orbit (°)**	**Avg. elevation in the area (°)**	**Avg. azimuth in the area (°)**	**Number of HD rain stations**
Astra 1L	SES	19.2 East	161	37.8	147
Hotbird 13F	Eutelsat	13 East	169	39.1	67
Astra 3B	SES	23.5 East	156	36.9	1

The OpenSat4Weather dataset includes measurements from 215 HD Rain stations, which are distributed as follows: 147 targeting the Astra 19.2°E (or Astra 1L) satellite, 67 targeting Hotbird 13°E (or Hotbird 13F), and 1 targeting Astra 23.5°E (or Astra 3B). Since these three satellites are located in a similar region of the sky, the elevation and azimuth angles of the satellite dishes are comparable across the stations (Table 2). Two hardware versions are present in the dataset: RBV2 (23

https://doi.org/10.5194/essd-2025-537
Preprint. Discussion started: 4 December 2025

Open Access Earth System Science Data Discussions

stations) and RBV3 (192 stations). RBV3 is the more recent model, providing the same measurements as RBV2, but featuring updated electronic components and a larger solar panel to improve autonomy. The stations are deployed at altitudes ranging from 0 to 1,622 m a.s.l., with a median altitude of 94 m and an average of 173.3 m. Each station collects data at two different frequency bands and two different polarizations. For each of the above four combinations, the Rainbox module measures the total RSL through the corresponding frequency band and polarization. The OpenSat4Weather dataset includes data from signals transmitted at horizontal polarization in the high-part of the Ku frequency band. This corresponds to the integration of the raw signal received from the satellite over the 11.70–12.75 GHz interval, that is, the band where the RSL is the strongest for the broadcasting satellites active in France. The station names follow the format “FRA-NNNNN”, where "FRA" represents the country code and "NNNNN" is the five-digit integer identifier of the station (e.g. “FRA-00002”).

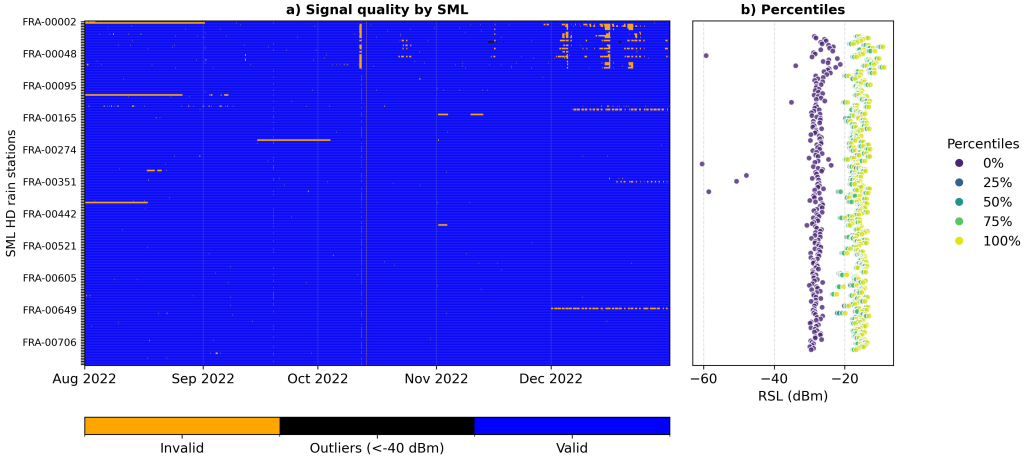

Figure 3. RSL data quality check for the 215 HD Rain SMLs during the five-month observation period. Each pixel on the left panel corresponds to a 1-minute time step for a station. Missing data (NA) are in orange, outliers, i.e., RSL values below -40 dBm, are in black, and values assumed to be problem-free are in blue. The right panel displays the RSL quantiles (in dBm) of each SML. SML are sorted by station ID in ascending numeric order from top to bottom.

The dataset consists of RSL time series in dBm recorded at a 1-minute temporal resolution with a precision of 0.01 dBm, and of the corresponding time stamps, expressed in UTC. The data cover the period from August 1 to December 31, 2022. Figure 3 shows a 2D picture of all the RSL samples labeled in three classes: missing values (NAs), outliers and valid data (Signal). It also reports a few RSL quantiles. The RSL values in the observation period and all the SMLs have a median of -16.4 dBm, a maximum of -8.8 dBm and a minimum of -60.5 dBm, respectively. The absolute value of the RSL is not a critical parameter as long as it remains within a given range, since it is directly affected by the antenna cable length between the dish and the Rainbox device. However, values that are too low (typically below -40 dBm) are generally suspect. These anomalously low values can be produced by different factors, such as a long antenna cable, which leads to additional signal loss, improper satellite alignment, defective LNB, etc. In any case, an analysis of the magnitude of the RSL must be always considered in

https://doi.org/10.5194/essd-2025-537
Preprint. Discussion started: 4 December 2025

relation to its variability over time. Only five stations in the dataset (FRA-00038, FRA-00309, FRA-00332, FRA-00348 and FRA-00375) recorded RSL values below -40 dBm, which can be considered outliers. The proportion of missing values (NAs) varies between 0.04% and 20.6% per station, with a median of 0.09% and a mean of 0.90%, respectively.

2.2 Rain gauges

The OpenSat4Weather dataset includes ground rainfall measurements collected by Météo-France's operational rain gauge network. These data are freely accessible via the Météo-France API portal or the open-data platform meteo.data.gouv.fr. Rain gauges undergo a data quality control process, which ends up in assigning one among the following quality codes (at every time stamp): "9 " denotes filtered data, "0" denotes protected data, that is, validated by manual inspection, "1" denotes validated data either by automatic procedure or by manual inspection, and, finally, "2" are questionable data (according to an automatic procedure).

The rain gauge dataset provides 6-minute rainfall accumulation measurements with a precision of 0.1 mm, covering the same period as the SML data (August 1 to December 31, 2022). A total of 113 rain gauges located within 10 km from every SML receiver locations were included. The rain gauges are installed at altitudes ranging from 1 m to 1464 m a.s.l., with median and mean altitudes of 184 m and 313 m a.s.l., respectively.

Figure 4 provides a summary of rain gauge sample statistics. It has the same format as Fig. 3. 41% (46) of the sensors contained invalid data, as shown in Figure 4a). The highest percentage of invalid data for a single sensor was 11.40%, with the average for affected sensors being 1.1%. Furthermore, zero rainfall was recorded in 86.7% to 99% of the 6-minute intervals, with the mean at 97.5%. The maximum recorded value is 26.9 mm in 6 minutes.

2.3 Weather radar

We used the rain gauge-adjusted weather radar product *Panthere* from Météo-France as an additional rainfall reference. The product is gridded with a spatial resolution of 1 km and a temporal resolution of 5 minutes. The data can be downloaded in real-time from Météo-France at https://portail-api.meteofrance.fr/web/fr/api/DonneesPubliquesPaquetRadar. The *Panthere* radar product is obtained from the data collected by the French radar network called ARAMIS. The network consists of 20 C-band radars, five S-band radars, six X-band radars and two radars deployed at airports in Paris and Nice (Chochon et al., 2022). A description of the methodology to derive the Panthere QPE product is available from Tabary et al. (2011). The above radar products do not have gaps in the period where SML data are provided.

We did not include the *Panthere* product as it is into the OpenSat4Weather dataset. Rather, we further processed the data to derive radar-based rainfall estimates in correspondence of each SML path, as detailed in Section 3.2, and included them into our dataset.

https://doi.org/10.5194/essd-2025-537
Preprint. Discussion started: 4 December 2025

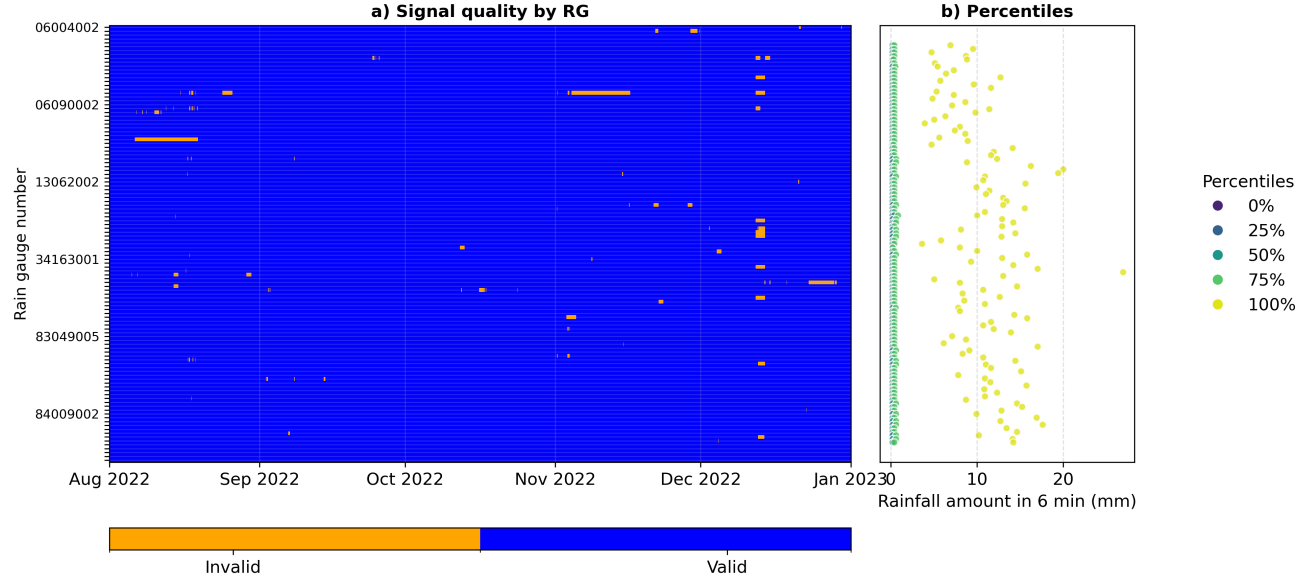

Figure 4. Rain gauge data quality check for the 113 sensors in the dataset. (a) Data labels (missing and valid samples), (b) Percentiles of 6-min rainfall depth, calculated from the set of non-zero measurements of each rain gauge time series. Rain gauges are sorted by station ID in ascending numeric order from top to bottom.

2.4 ERA5

The knowledge of the 0°C isotherm is essential to identify the rain height, i.e., the height of the part of the link where liquid precipitation occurs. Here we use ERA5, a global scale reanalysis atmospheric dataset, which is available at the Copernicus Climate Data Store. (https://cds.climate.copernicus.eu/datasets). The ERA5 products are derived from the integrated forecast model, elaborated by the European Centre for Medium-Range Weather Forecasts (ECMWF), by assimilating a number of meteorological observations from different sources. The ERA5 single-layer data include the 0°C isotherm height with hourly temporal resolution and 0.25° spatial resolution (i.e. about 28 km). The above variable represents the height (in meters above sea level) where the temperature of the air reaches 0°C. This, in turn, is crucial for identifying the melting layer height, that is, the height above sea level where solid particles have melted into raindrops, as shown in Section 3.1.

3 Data preparation (Methods)

This section describes how the raw data in the datasets listed in previous Section 2 have been manipulated before being stored into the OpenSat4Weather dataset. In particular, the ERA5 temperature data have been processed to extract the information on rain height (Section 3.1). The radar data have been spatially aggregated to provide rainfall estimates comparable to the ones

https://doi.org/10.5194/essd-2025-537
Preprint. Discussion started: 4 December 2025

Open Access Earth System Science Data Discussions

that can be extracted from the SML data (Section). Finally, the dataset format and structure are briefly described in Section 3.3.

3.1 Rain height

Even though a discussion of the methods for retrieving rainfall intensity from SML raw data is beyond the scope of this paper, nonetheless it is important to understand the role of rain height in SML data processing. The standard conversion formula between rainfall intensity R (in mm/h) and rain attenuation γ per unit length is given by ITU-R P.838-3 (2005)

$$\gamma = \kappa R^{\alpha} \quad \text{dB/km} \tag{1}$$

where κ and α are coefficients dependent on SML signal frequency and polarization and on the link elevation angle. If the path goes through a rain layer with a vertical extent equal to h_R km with an elevation angle θ, R can be estimated as follows

$$R = \left(\frac{A}{\kappa} \cdot \frac{\sin\theta}{h_R} \right)^{1/\alpha} \quad \text{mm/h} \tag{2}$$

where A is the RSL attenuation (dB) across the rainy layer detected by the SML. Equation (2) assumes that rain is uniform along the rainy path up to h_R and that there are no other relevant sources of attenuation besides rain. Both assumptions are not true in practice, hence h_R is often considered as an effective rain height rather than the physical height up to which liquid particles are found. The (physical) rain height can be determined by weather radar measurements. Radars detect the presence and the height of the melting layer, which looks like a thin vertical layer of enhanced reflectivity (namely, the bright band), located just below the 0°C isotherm and produced by backscattering through snowflakes melting into raindrops (Thurai et al., 2003). Hence, the top of the bright band is the 0°C isotherm height, whereas the bottom of the bright band is the physical rain height. Alternatively, h_R can be determined by models. For instance, ITU-R P.839-4 (2013) statistical model predicts the mean annual rain height above mean sea level from the mean annual 0°C isotherm as

$$h_R = h_0 + 0.36 \quad \text{km} \tag{3}$$

The above is an effective rain height that can be used to predict rain attenuation across an Earth-satellite path on a statistical basis. The rain height includes not only the contribution of liquid precipitation to path attenuation but also the one of the melting layer. Furthermore, (3) is an average between stratiform and convective precipitation. The former is generally associated with large spatial scales, low-intensity values and a well-defined layered vertical structure (a frozen layer, a melting layer and a liquid precipitation layer). Convective precipitation is characterized by vertical winds (downdrafts and updrafts), which generate high-intensity localized phenomena, and does not exhibit a clear separation between frozen and liquid phase. Radar observations show that the 0°C isotherm stands 200-300 m above the bright band (Thurai et al., 2005), when the latter is visible and, in some cases, even 500 m above it. The rain height during convective events can extend much above the 0°C isotherm level when strong updrafts are detected, even though the vertical distribution of rain is not uniform. Capsoni et al. (2009) proposed a more refined statistical method then the one in (3) to calculate separate values of h_R for stratiform and convective rain, including the contribution of the melting layer, based on a weighted average of monthly mean values of the 0°C isotherm.

https://doi.org/10.5194/essd-2025-537
Preprint. Discussion started: 4 December 2025

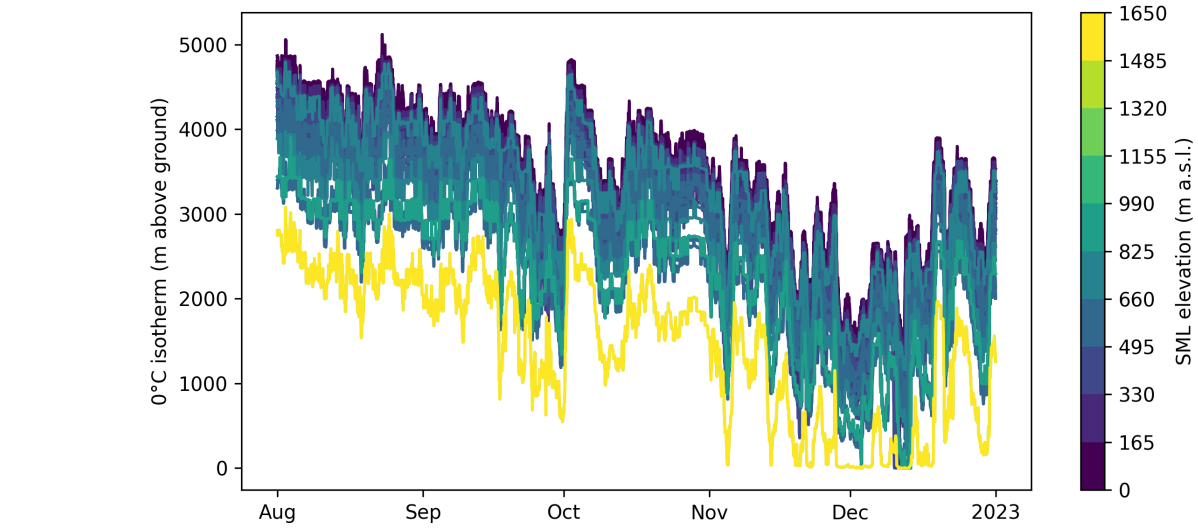

Figure 5. Time series of the 0°C isotherm height (in meters above sea level) from August 2022 to December 2023, extracted from ERA5 reanalysis data. Each line represents the isotherm height over time at the ERA5 grid point corresponding to the location of an SML receiver. Line colors indicate the elevation of SML receivers, highlighting the dependence of isotherm variability on receiver altitude and seasonal atmospheric changes.

In principle, (3) and other statistical methods should not be used to derive rainfall intensity from the time series of SML raw data, as the 0°C isotherm as well as the rain height have a seasonal and, possibly, a daily variability. Weather radar data, radiosoundings or, again, the outputs of Numerical Weather Prediction (NWP) models should be used instead, when available. Once the current value of the 0°C isotherm and of the (physical) rain height are known, a two-layer model (melting layer + liquid layer) as the one in (Giannetti et al., 2019) can be used at least for stratiform precipitation, to estimate the rainfall intensity at a certain time instant, under some conditions. Time series of the 0°C isotherm height for each SML are provided in the OpenSat4Weather dataset. These data were retrieved from ERA5 reanalysis and are presented in Figure 5. For each SML, the ERA5 grid cell corresponding to the SML receiver location was selected to approximate the atmospheric profile along the link path. However, it should be noted that the spatial resolution of ERA5 is not optimal to fully resolve fine-scale topographic or meteorological variations. In some cases, multiple SML receivers fall within the same ERA5 grid cell, resulting in identical 0°C isotherm time series despite differences in receiver altitudes. As shown in Figure 5 the 0°C isotherm exhibits significant temporal and spatial variability, driven by both seasonal changes and the altitude of the terrain. The general trend shows a gradual decrease of the 0°C isotherm height from late summer to winter, with peak values exceeding 5000 m above ground in August and minimum values reaching 360 m above ground. This variability is critical in the context of rainfall retrieval from SMLs, as it affects the estimation of the effective rain height. The color gradient in the figure, representing the elevation of the SML receiver locations, further emphasizes how lower-altitude areas tend to show a reduced 0°C isotherm height.

https://doi.org/10.5194/essd-2025-537
Preprint. Discussion started: 4 December 2025

3.2 Radar-based rainfall along SML path

We built up the radar-based estimate of rainfall intensity in correspondence of each SML path according to the rationale described hereinafter. We used the grid intersection method from poligrain (https://github.com/OpenSenseAction/poligrain) to compute the length of each SML path in the transecting radar pixels. As the SML rainfall estimate depends on the melting layer height, we calculated the intersections between radar pixels and SML path for melting layer heights between 0 and 6000 m above ground in 250 m steps. Each grid cell intersected by the SML path was assigned a weight based on the length of the path segment within that cell. For each time step in the SML dataset, the current height of the melting layer was used to calculate all intersected pixels. Finally, rainfall values from all intersected grid cells were averaged, with each cell's value weighted according to the above intersection weights. Thus, we derived a radar reference that matches the actual measurement of the SML through the rainfall in the atmosphere from the location of the SML receiver to the point where the SML path reaches the melting layer. An example of the radar-based rainfall intensity along an SML path is shown in Section 4.

3.3 Data format

One issue with opportunistic data is that there are not standardized procedures for generating, formatting and storing the data. However, a recent paper contributed to fill the gap, recommending data format conventions for different types of opportunistic data, including SMLs (Fencl et al., 2024). The above work is the result of the activity carried out by the researchers involved in the COST Action named OpenSense (Opportunistic Precipitation Sensing Network), which aims to improve access to opportunistic precipitation observations (https://opensenseaction.eu/). The format for data storage recommended by (Fencl et al., 2024) is *NetCDF*, basically due its flexibility and portability. The authors also provided a set of conventions for variable and metadata naming. Finally, their specifications distinguish between required and optional data and metadata elements to ensure consistency and interoperability across datasets. The OpenSat4Weather dataset follows the above recommendations, including all the required SML data.

The dataset include the following three *NetCDF* files:

- *SML_data_2022.nc*: stores SML data
- *radar_along_SML_data_2022.nc*: stores radar data
- *rg_data_2022.nc*: stores rain gauge data

The *SML_data_2022.nc* file hosts the following variables:

- The main variable is the RSL, stored in the file with the dimensions *sml_id* and *time*
- The variable *deg0l* represents the 0°C isotherm height at the loaction of the HD Rain stations. The hisotherm data are extracted from ERA5 reanalysis data.
- The required metadata consists of the following variables:

https://doi.org/10.5194/essd-2025-537
Preprint. Discussion started: 4 December 2025

- SML ID
- time
- frequency
- coordinates and height above sea level
- azimuth and elevation angle.
- name of the satellite the SML is pointing at

The radar along the SML path reference is stored with the same dimensions, format and naming convention as the SML data itself. The meta data of the SML are not included and the variable is called *rainfall_amount*. The rain gauge station data contains the variable *rainfall_amount* with time, coordinates and the height above sea level.

4 Results

Figure 6 presents an example time series of RSL collected by SML FRA-00332 (43.556° N, 6.967° E, 9 m amsl) and corresponding meteorological data for 15-Dec-2022. Panel a) displays the 1-minute resolution RSL, showing a prolonged rain event from 07:00 to approximately 23:00, with a peak between 16:00 and 17:00. At this rainfall peak, the RSL drops by about 10 dB. Panel b) illustrates hourly aggregated rainfall intensity profiles from nearby rain gauge and radar. These profiles generally correlate well with each other and with the RSL. We remind the reader that the radar data are interpolated along the projection on ground of the SML rainy path. While all three sensors capture the precipitation peak, the radar indicates a smaller peak intensity compared to the rain gauge. Moreover, the minimum of the RSL profile is delayed with respect to the rainfall peak as observed by the radar. Panel c) shows the 0°C isotherm time series from ERA5 data, which drops by approximately 200 m during the event, influencing the rainy path length.

Fig. 7 shows the descriptive statistics of rainfall during the five month observation period, gathered from the 113 Météo-France rain gauges located in the area where SMLs are deployed. The rain gauges are sorted from left to right in order of increasing elevation above sea level. The following four quantities are plotted for each rain gauge, aggregating the original 6-min rainfall accumulation into hourly periods, as suggested by (Andersson et al., 2022): a) wet fraction, b) total rainfall accumulation in the period, c) maximum value of the hourly accumulation, and d) standard deviation of the hourly accumulation (wet hours only). An hourly period is flagged as wet if the accumulation exceeds 0.1 mm. The wet fraction is comprised between 3.8% and 7.5% of time in 90% of cases. The total accumulation in the period goes from about 204 to 526 mm in 90% of cases. The data highlight a weak trend towards the increase of wet percentage and of rain accumulation with the elevation.

4.1 Descriptive Analysis of SML data

Figure 8 shows basic statistics per SML link, computed over the entire period. The first boxplot represents, for each link (y-axis), the median values (orange line) and several quantiles in dBm. In this Figure 8, links are ordered by altitude (from lowest on the left to highest on the right). At first glance, there appears to be no clear relationship between received power and

https://doi.org/10.5194/essd-2025-537
Preprint. Discussion started: 4 December 2025

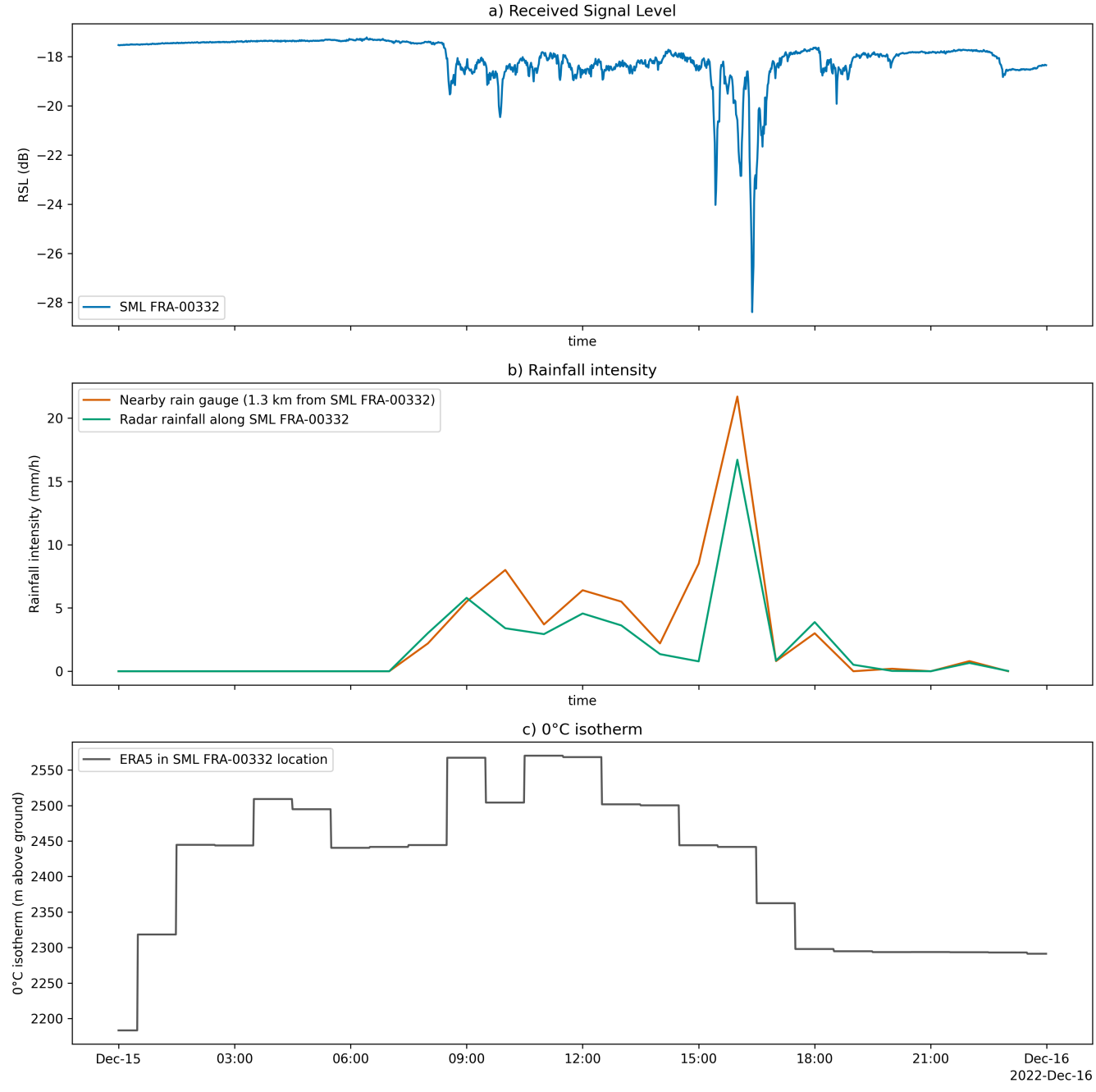

Figure 6. Example time series of RSL (a) from SML FRA-00332 (43.556° N, 6.967° E, 9 m amsl), with corresponding rainfall intensity from rain gauge and radar (b), and °C isotherm from ERA5 (c), for 15-Dec-2022.

https://doi.org/10.5194/essd-2025-537
Preprint. Discussion started: 4 December 2025

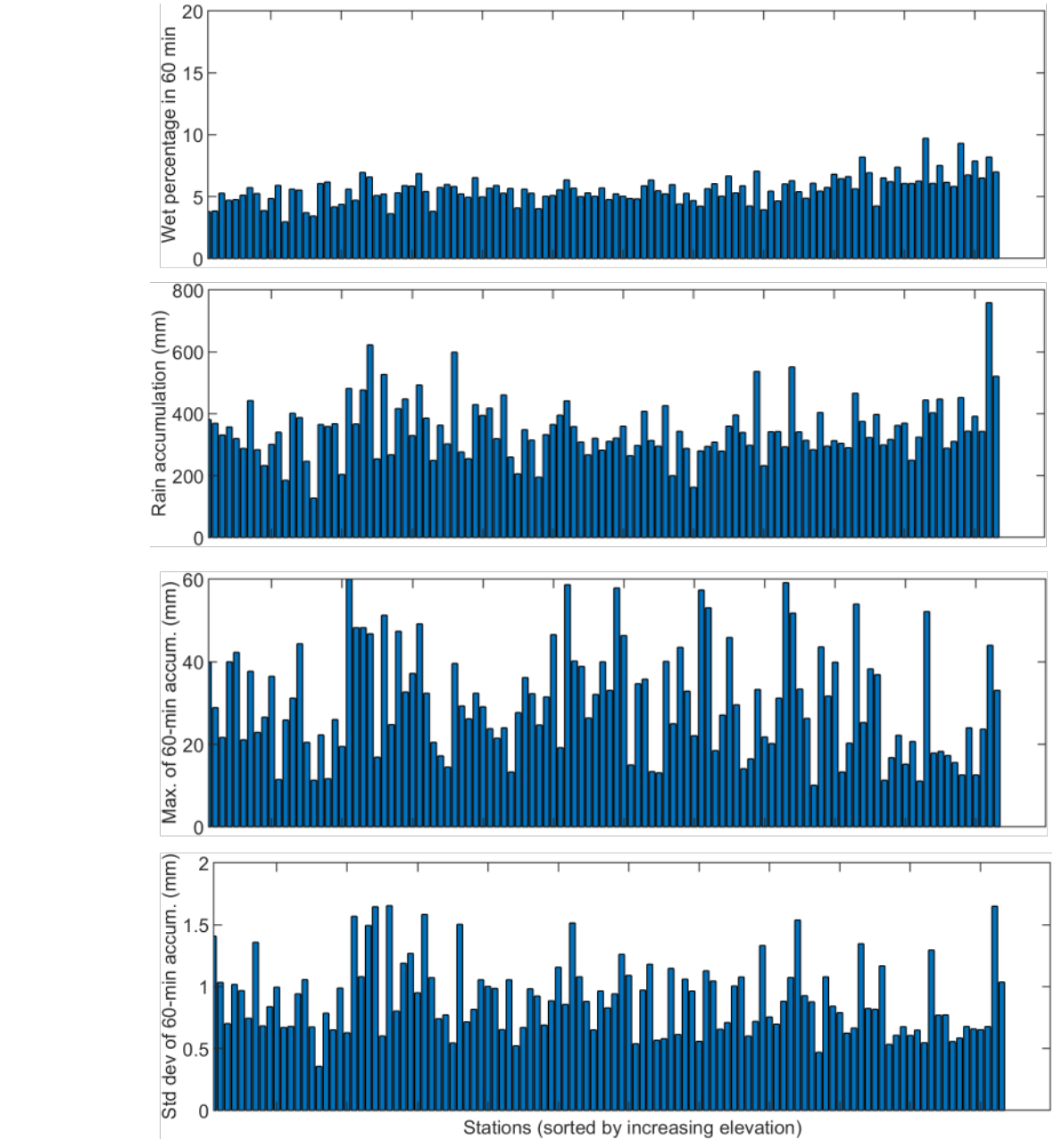

Figure 7. Descriptive statistics of rainfall collected by the 113 available rain gauges during the five-month observation period.

altitude. Median received powers vary greatly, ranging from –24 to –10 dBm. While particularly low values may sometimes indicate malfunction, one should not jump to conclusions: the main factor affecting average received power is the length of the coaxial cable used during installation. Longer cables induce greater losses, which shift the signal downward without

https://doi.org/10.5194/essd-2025-537
Preprint. Discussion started: 4 December 2025

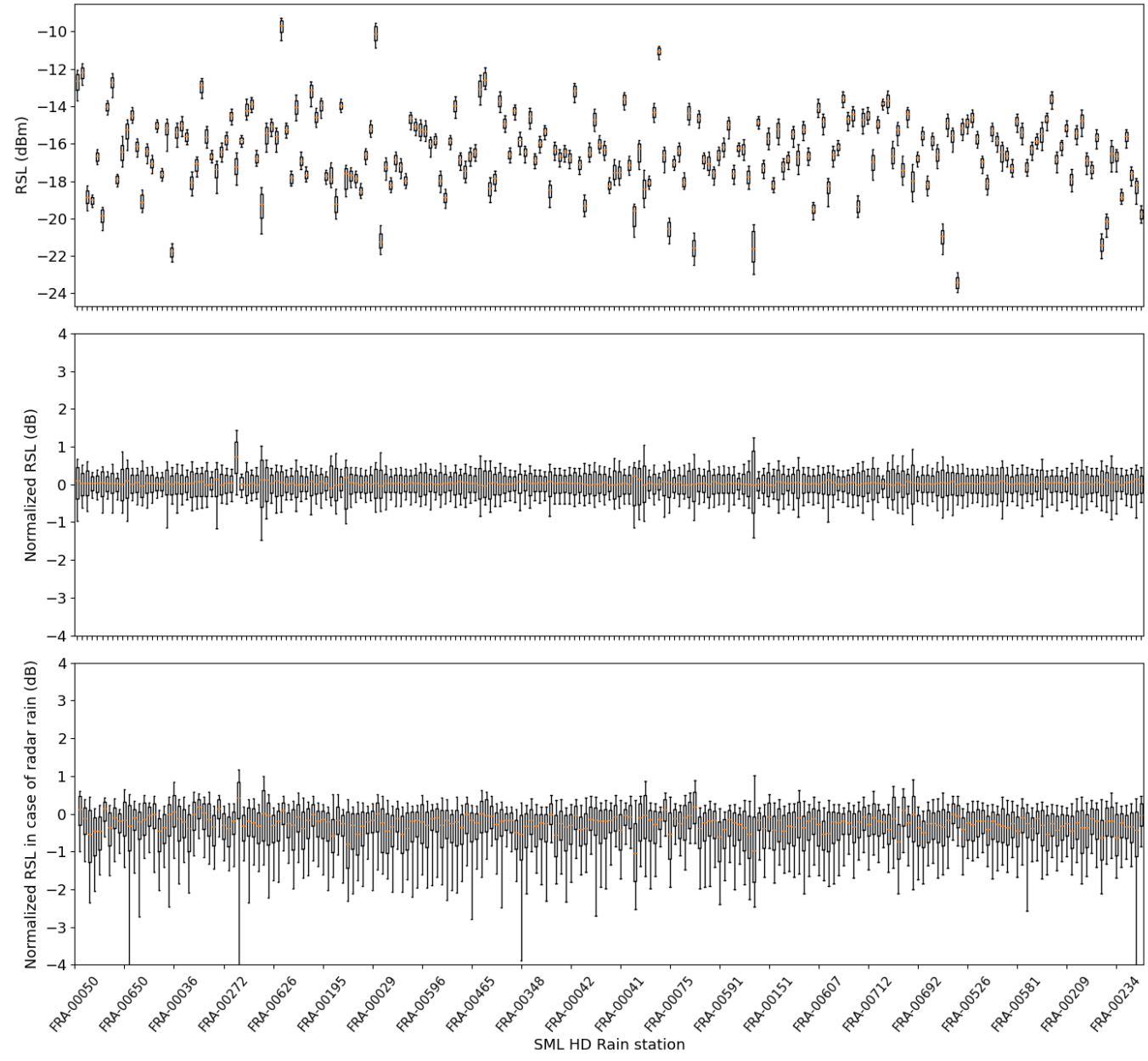

Figure 8. Descriptive statistics of SML data. Each box (x-axis) corresponds to an SML link. In all cases, the statistics are computed over the entire five-month period at 5-minute resolution: the median (orange horizontal line), the 25% and 75% quantiles (box), and the 5% and 95% quantiles (vertical lines). Top: received signal level (dBm). Middle: received signal level normalized to its mean value for each link (dB). Bottom: same as above, but restricted to the time steps where radar detects a rainfall accumulation greater than 0 mm (dB).

https://doi.org/10.5194/essd-2025-537
Preprint. Discussion started: 4 December 2025

necessarily compromising its quality. Therefore, analysis should focus on relative signal drops (e.g., due to rain) rather than absolute values, which are highly variable.

To highlight some visual patterns without using advanced algorithms (e.g., baseline detection), we simply normalized each link by subtracting its mean received power over the period. The second boxplot in Figure 8 illustrates this. Here, the boxplots are centered around 0 dB. A few links stand out—either because they are shifted (indicating a few extreme values affecting the mean but not the quantiles) or because they exhibit higher variability. This is a strong indicator of malfunctioning links. However, such cases are rare: for the vast majority, 90% of the values (represented here by the 5% to 95% quantiles) fall within a range of about 1.5 dB. This suggests that rainfall(especially heavy rainfall which typically induces signal attenuations above 1 dB) is not strongly visible in this representation. This is not surprising: radar data projected onto the SML link footprints show rainfall occurrence between 3.2% and 7.4% of the time at 5-minute resolution, barely within the represented quantile range. Furthermore, a large share of these rainy periods corresponds to light rainfall, which would in any case produce attenuation below 1 dB. For instance, only 26% of rainy timestamps (5-minute resolution) show rain rates above 2 mm/h according to radar data over the SML link paths.

The third boxplot in Figure 8 shows the same normalized data, but restricted to time steps where radar along each link's path detects positive rainfall. This time, the effect of rain is clearly visible. Although the median is only slightly affected (generally between –1 and 0 dB), the lower quantiles (25% and 5%) drop significantly—across almost all stations—and variability increases, similarly to the radar data (with total accumulations ranging from 230 to 727 mm depending on the link). Again no clear altitude effect appears on this boxplot.

Figure 9 presents statistics derived from radar and SML data, but this time across all SML links and in the form of time series. In the top plot, we show the average of the RSL values normalized per link (in green), along with the 95th percentile (links receiving the strongest signal at a given time relative to their own mean, in blue) and the 5th percentile (weakest signals, in red). For comparison, we also display the average radar rainfall (in black) over all SML link paths. The two lower plots are zoom-ins on two 10-day periods.

We observe that during dry weather, there is a clear day/night alternation in the signal, which we will discuss later. This effect is especially pronounced in summer (i.e., at the beginning of the observation period). Rainfall periods are clearly visible, particularly in the 5th percentile. In the September zoom-in, the 5th percentile drops sharply (nearly –3 dB), while the 95th percentile remains unaffected and the mean only slightly decreases. This suggests heavy but localized rainfall over part of the French Mediterranean arc. In contrast, during the December period, the 5th percentile is less impacted (no more than –1.5 dB attenuation), but even the 95th percentile drops slightly—indicating more widespread but less intense rainfall.

4.2 SML - rain gauge association

The geographical distribution and proximity of rain gauges to SML sensors are crucial for effectively leveraging opportunistic data, as the distance to the nearest rain gauge directly impacts comparative analysis for validation. Figure 10 illustrates, through boxplots, the distribution of distances to the three closest rain gauges for all 215 HD Rain stations. In our dataset, the average distance to the closest rain gauge is 5.87 km, with an interquartile range (IQR) of 5.16 km (25th percentile: 3.13 km, 75th

https://doi.org/10.5194/essd-2025-537
Preprint. Discussion started: 4 December 2025

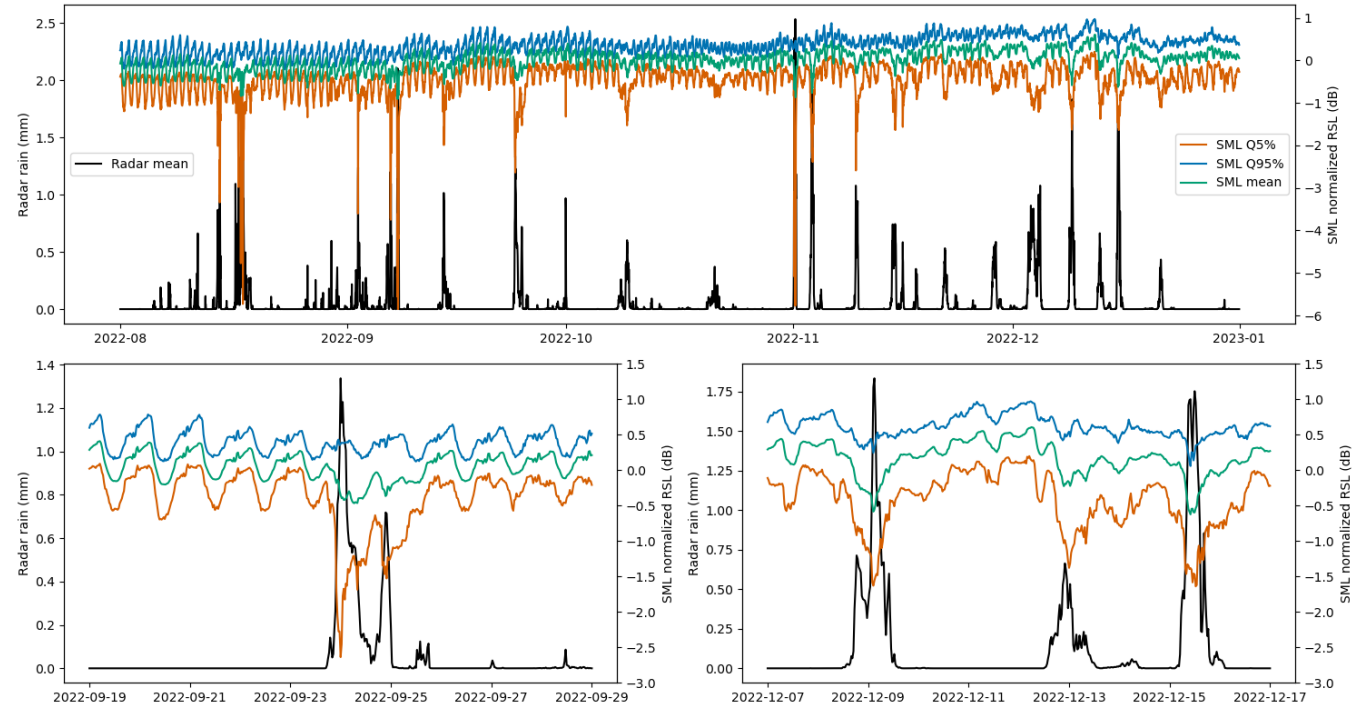

Figure 9. Temporal evolution from August to December 2022 of radar and SML data. Top: full period. Bottom: zoom on two 10-day periods. Green: average of all links' RSL values normalized by their link-specific mean; Blue: same for the 95% quantile (high values); Red: same for the 5% quantile (low values). Black: average radar rainfall accumulation over the SML link footprints, in mm.

percentile: 8.29 km), and values ranging from a minimum of 0.06 km to a maximum of 19 km. For the second and third closest gauges, the mean distances are 10.43 km and 13.93 km, respectively, with interquartile ranges of 5.10 km and 6.76 km. Overall, 43% of SMLs have their closest rain gauge within 5 km, and this percentage rises to 87% within a 10 km radius, indicating a relatively homogeneous distribution of rain gauges and HD Rain stations across the territory.

4.3 Analysis of the radar along SML-path based on ERA5 melting layer

There is a large variation of the melting layer height estimated by ERA5 over the observation area from over 5000 m above sea level in August to less than 1000 m in December. In general, the melting layer usually lies above 2000 m from August to mid-October. This results in an average SML path length of about 6000 m before reaching the melting layer. From November on, the path length of the SMLs is generally below 3000 m.

Figure 11 shows the altitude of the 0°C isotherm from August to December 2022 (bottom), along with the signal received by one of the SML links (top, in dBm), and rainfall intensities measured along the link path by a weather radar and by a nearby rain gauge (middle, in mm/h). Severe signal attenuation (around 12 dB) is observed in summer during heavy rainfall events, with 0°C isotherm altitudes being around 4 km. Around late October to early November, another combination of intense rainfall

https://doi.org/10.5194/essd-2025-537
Preprint. Discussion started: 4 December 2025

Open Access Earth System Science Data Discussions

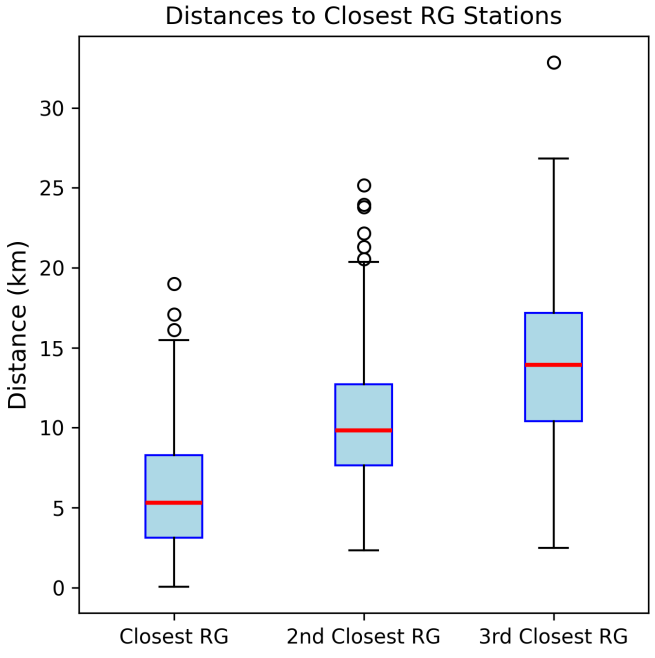

Figure 10. Boxplots representing the distribution of distances between HD Rain stations and their three nearest rain gauges.

(40 to 50 mm/h), large attenuation (around 10 dB), and high 0°C isotherm altitude (around 3500 m) is observed. Later in the period, as the atmosphere cools, we see weaker rainfall events (10 to 25 mm/h) in early December, with lower 0°C isotherm heights (1500–2000 m), leading to much smaller attenuation values (around 1 dB).

This highlights a clear seasonal pattern in temperate regions: stronger rainfall tends to occur during warmer periods, when the 0°C isotherm is high, which results in stronger attenuation, due both to higher specific attenuation and a longer integration path through the rainy layer. Conversely, in winter, rainfall is often weaker (typically stratiform), with a lower 0°C isotherm height, thus, it produces a much lower attenuation. This seasonality may complicate rainfall estimation: in summer, strong attenuation can lead to saturation (complete signal loss), while in winter, the low variability in signal can make it harder to detect and estimate rainfall reliably, as the baseline becomes more difficult to identify.

However, these patterns are not universal. In the Mediterranean regions, for example, intense rainfall events can occur during colder months, while stratiform rainfall may appear in summer.

Finally, it is worth noting that the 0°C isotherm exhibits substantial variability, not only at seasonal scale but also at shorter time scales: changes of 1–2 km can occur over just a few days. For instance, 0°C isotherm above 3000 m can still occur in late December, while values below 2500 m are already present in early October. This variability calls for the use of dynamic 0°C isotherm data (rather than climatological averages), such as those provided by ERA5 reanalyses or by numerical weather predictions if real-time operation is needed.

https://doi.org/10.5194/essd-2025-537
Preprint. Discussion started: 4 December 2025

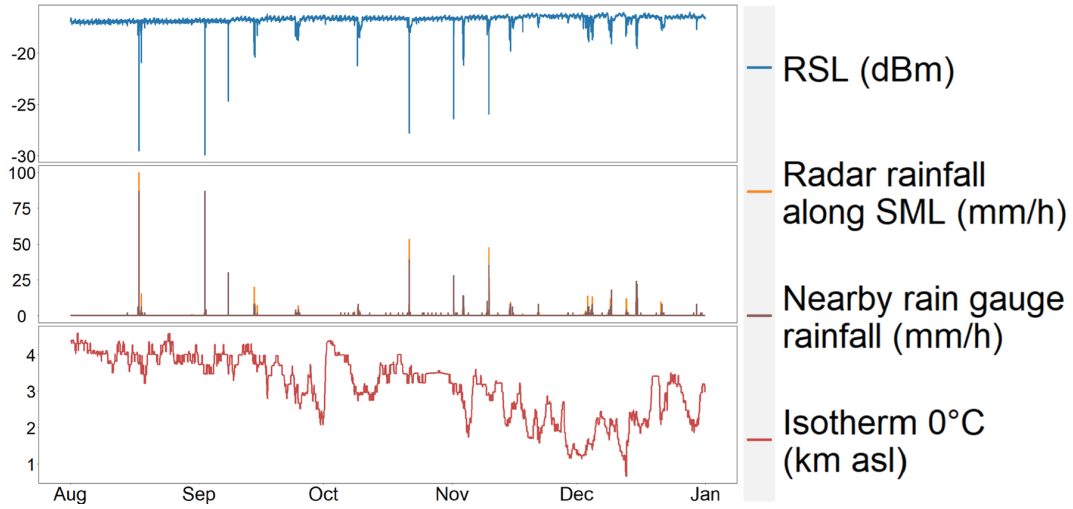

Figure 11. RSL signal (dBm) of the SML FRA-00410 (top), rainfall (mm/h) from corresponding pixels radar and the closest rain gauge (middle), and the isotherm 0°C height above sea level for the location that SML (bottom) are shown.

5 Discussion

As seen previously in Figure 6, the RSL variation is strongly linked to rain intensity. However, other effects can have a non-negligible impact on the signal. Furthermore, hardware limitations and malfunctioning of the ground terminal may result in noticeable RSL patterns. These effects should be accounted for and canceled, if possible or, at least, identified, to avoid misclassify such RSL variations as rain events.

For example, temperature significantly affects the RSL. Figure 12 shows clear variations in the signal that are inversely correlated with the temperature increase on November 16, and 17, and, to a lesser extent, on November 13 and 18. This variation is specific to sunny days where the temperature notably changes between night and day. One possible explanation is a temperature-dependent variation in the LNB gain. The sharp and relatively short drops on November 14, late in the day on November 15, and during the night of November 17-18 are rain events.

Temperature is not the only factor affecting the signal. Effects of the interaction between raindrops and the systems characteristics can also impact the quality of the received signal, making its interpretation not straightforward for conversion into rainfall data, as shown in Figure 13. Panel a) shows the time series relative to a rainy day. The RSL is strongly correlated with the the profile of the rainfall intensity measured by the radar (and calculated along the SML path). Rain stops at noon. However, from this moment on, the RSL slowly increases only to get back to its level before the rain event after several hours. This signal pattern is likely due to the gradual drying of the antenna after the rain event. This phenomenon is similar to the "wet antenna" effect observed in CMLs by several authors (see e.g. (Leijnse et al., 2007b)). Panel b) highlights a short segment of an RLS time-series. The almost flat plateau visible from 12:25 to 12:35 corresponds to the received signal dropping below the minimum detectable signal by the LNB during intense rain. For this station, the maximum measurable attenuation is 14 dB.

https://doi.org/10.5194/essd-2025-537
Preprint. Discussion started: 4 December 2025

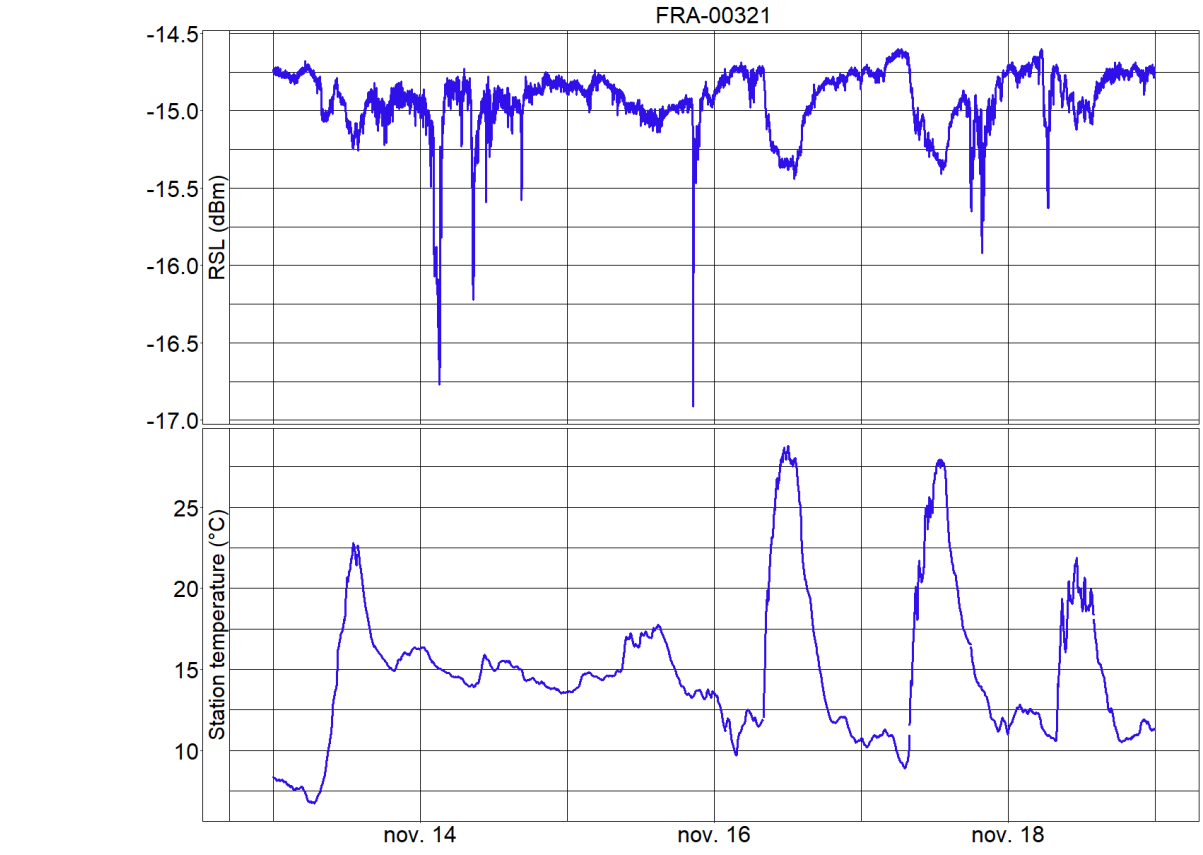

Figure 12. An example of RSL (dBm) pattern and corresponding temperature (°C) measurements. Station: FRA-00321.

Beyond this limit, the signal cannot be distinguished by noise. It is important to note that this maximum measurable attenuation is not equal to the clear-sky signal-to-noise ratio, but it is actually less than that, because the noise level significantly increases during rain. This effect is produced by the raindrops, which behave as radiating bodies. A small but not negligible fraction of this energy is irradiated in the microwave spectrum and it is captured by the antenna of the SML, hence producing an additional noise contribution. Typically, with a signal-to-noise ratio of around 18 dB, the maximum measurable rain attenuation is around 14 dB, related to an increase in the background noise of about 4 dB (Gelbart et al., 2025). This maximum SNR in clear-sky depends on the targeted satellite (transmit power level), on the size of the receiving dish (assuming optimal alignment), and, to a lesser extent, on the quality of the dish and on the LNB. The anomalous pattern in panel c) indicates an issue with the cable connecting the antenna to the LNB, which results in a complete signal loss (RSL around -60 dBm), making the signal unusable. Finally, panel d) shows two signal drops occurred in mid-September and in late November produced by a misalignment of the TV dish and caused by wind or other factors.

https://doi.org/10.5194/essd-2025-537
Preprint. Discussion started: 4 December 2025

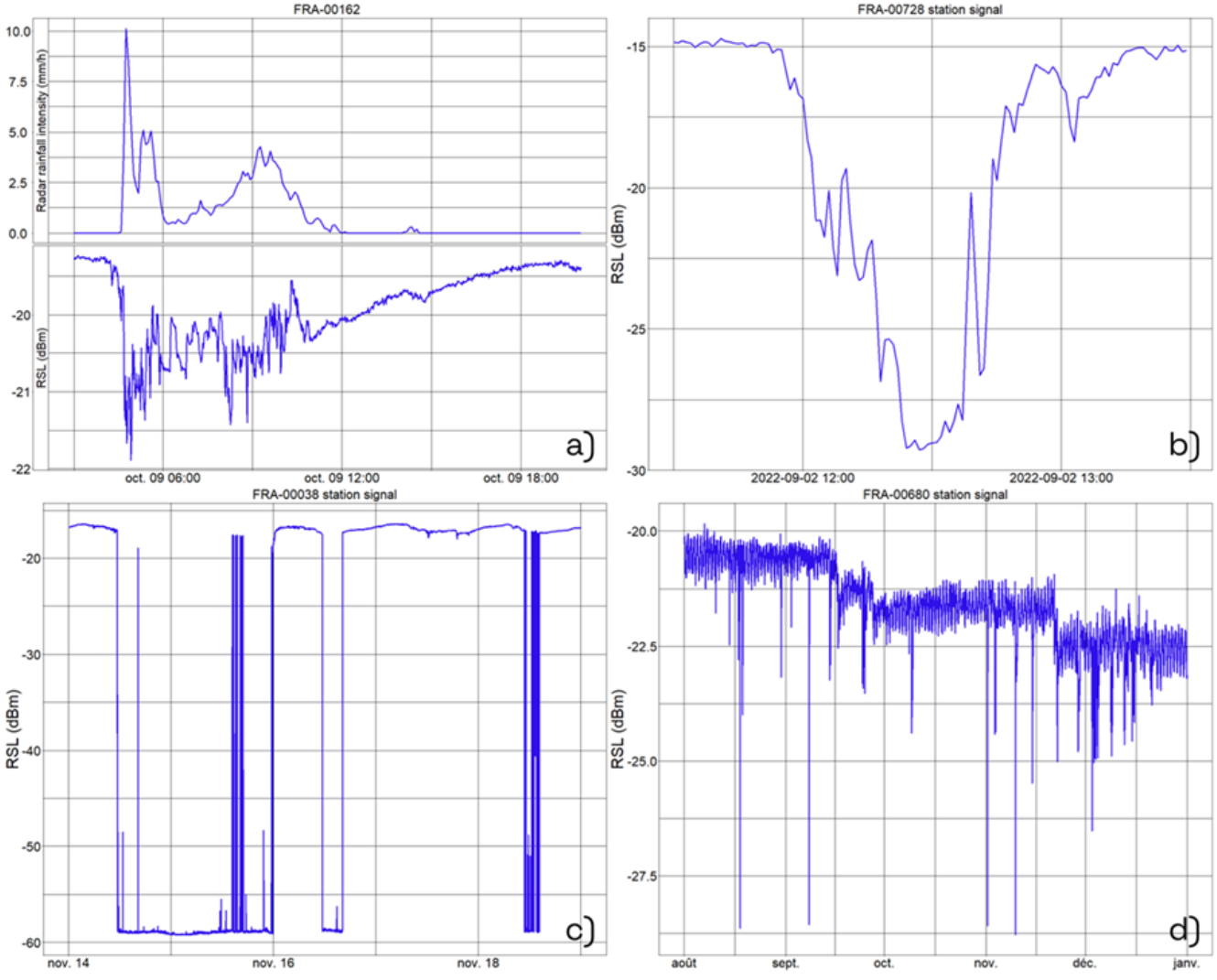

Figure 13. Examples of disturbances and anomalous RSL patterns a) sensor humidification after a rainfall event. b) saturation during an intense rainfall event. c) LNB cable disconnection. d) multiple misalignments of the dish over time.

Through these examples, it is clear that the signal varies with rain intensity, but numerous other parameters can cause signal variations, making it more difficult to isolate the rain's contribution. Therefore, using neural networks for this task seems particularly relevant, as they are well-suited to identify the amplitude, duration, and frequency of rain-induced disturbances (Gianoglio et al., 2024).

https://doi.org/10.5194/essd-2025-537
Preprint. Discussion started: 4 December 2025

6 Conclusions

We presented the OpenSat4Weather open access dataset, which provides SML data aimed at the opportunistic sensing of precipitation. The data are the raw time series of RSL collected by the low cost receivers used for TV-SAT service reception. SMLs are easy to deploy, they have limited power consumption and data can be transferred from the sensors to a remote server by a Wi-Fi or 4/5G network, hence they are suitable to monitor precipitation in areas where convectional sensors are scarce or unavailable.

RSL data for 251 SML sensors operating in the ku-band and located in southern France are included in OpenSat4Weather. The data are sampled once every 1-min and extend over a five month observation window (August-December 2022). The metadata (i.e. ground station coordinates, and satellite identifier, elevation and azimuth) are provided as well. The SMLs in the dataset work with horizontal polarizations and the RSL should be considered a 1-min average of the signals received across the higher part of the ku-band, i.e. 11.70-12.75 GHz. Moreover, the dataset includes corresponding time series of the 0°C isotherm height along each satellite-to-ground path at hourly intervals, which allow to quantify the length of the rainy part of the propagation path. The latter, in turn, is used in the conversion process of RSL into rainfall intensity. Finally, OpenSat4Weather features conventional rainfall data collected by rain gauges and weather radars that can be used for comparison and validation studies as well as into the RSL data processing chain, for instance for determining wet and dry periods of time.

The data are stored in the Netcdf format, which is supported by most of the computing platforms used by scientists and engineers. The dataset is openly available on zenodo. OpenSat4Weather fulfills the guidelines for FAIR data (namely, Findable, Accessible, Interoperable and Reusable) (Wilkinson et al., 2016)

7 Data availability

The OpenSat4Weather dataset is openly available at https://doi.org/10.5281/zenodo.16530166 under the Creative Commons Attribution Share Alike 4.0 licence (Nebuloni et al., 2025). More details on the data structure and files are provided in the data repository. The OpenSat4Weather data covers the period August–December 2022. Additional data from the Météo-France ground weather stations can be downloaded at https://meteo.data.gouv.fr/ (last access: 31 July 2025)

Author contributions. RN and MG conceived the idea and reached the agreement with data owners to openly share the SML dataset. MG and GC collected rain gauge, weather radar and ERA5 data, and converted these data as well as SML data into the NetCdf format. FM and MT analyzed the SML data. RN analyzed the rain gauge data. MG analyzed the radar data. GC analyzed the ERA5 data. All the authors contributed to write and review the manuscript.

Competing interests. The contact author has declared that none of the authors has any competing interests.

https://doi.org/10.5194/essd-2025-537
Preprint. Discussion started: 4 December 2025

Acknowledgements. This work has been carried out within the framework of the COST Action OPENSENSE, CA20136, "Opportunistic Precipitation Sensing Network" supported by COST (European Cooperation in Science and Technology). The authors thank Sereno/HD Rain company for sharing their SML data and Meteo France for providing open access to their meteorological products.

https://doi.org/10.5194/essd-2025-537
Preprint. Discussion started: 4 December 2025

References

Adirosi, E., Facheris, L., Giannetti, F., Scarfone, S., Bacci, G., Mazza, A., Ortolani, A., and Baldini, L.: Evaluation of Rainfall Estimation Derived From Commercial Interactive DVB Receivers Using Disdrometer, Rain Gauge, and Weather Radar, IEEE Transactions on Geoscience and Remote Sensing, 59, 8978–8991, https://doi.org/10.1109/TGRS.2020.3041448, 2021.

Andersson, J. C. M., Olsson, J., van de Beek, R. C. Z. ., and Hansryd, J.: OpenMRG: Open data from Microwave links, Radar, and Gauges for rainfall quantification in Gothenburg, Sweden, Earth Syst. Sci. Data, 14, 5411–5426, https://doi.org/10.5194/essd-14-5411-2022, 2022.

Angeloni, S., Adirosi, E., Sapienza, F., Giannetti, F., Francini, F., Magherini, L., Valgimigli, A., Vaccaro, A., Melani, S., Antonini, A., and Baldini, L.: Enhanced Estimation of Rainfall From Opportunistic Microwave Satellite Signals, IEEE Trans. Geosci. Remote Sens., 62, 1–12, https://doi.org/10.1109/TGRS.2023.3349100, 2024.

Arslan, C. H., Aydin, K., Urbina, J. V., and Dyrud, L.: Satellite-link attenuation measurement technique for estimating rainfall accumulation, IEEE Transactions on Geoscience and Remote Sensing, 56, 681–693, 2017.

Barthès, L. and Mallet, C.: Rainfall measurement from the opportunistic use of an Earth–space link in the Ku band, Atmospheric measurement techniques, 6, 2181–2193, 2013.

Capsoni, C., Luini, L., Paraboni, A., Riva, C., and Martellucci, A.: A New Prediction Model of Rain Attenuation That Separately Accounts for Stratiform and Convective Rain, IEEE Transactions on Antennas and Propagation, 57, 196–204, https://doi.org/10.1109/TAP.2008.2009698, 2009.

Chochon, R., Martin, N., Lebourg, T., and Vidal, M.: Analysis of extreme precipitation during the mediterranean event associated with the Alex storm in the Alpes-Maritimes: atmospheric mechanisms and resulting rainfall, pp. 397–418, 2022.

Colli, M., Stagnaro, M., Caridi, A., Lanza, L. G., Randazzo, A., Pastorino, M., Caviglia, D. D., and Delucchi, A.: A Field Assessment of a Rain Estimation System Based on Satellite-to-Earth Microwave Links, IEEE Trans. Geosci. Remote Sens., 57, 2864–2875, https://doi.org/10.1109/TGRS.2018.2878338, 2019.

Colli, M., Cassola, F., Martina, F., Trovatore, E., Delucchi, A., Maggiolo, S., and Caviglia, D. D.: Rainfall Fields Monitoring Based on Satellite Microwave Down-Links and Traditional Techniques in the City of Genoa, IEEE Trans. Geosci. Remote Sens., 58, 6266–6280, 2020.

Covi, E. and Roversi, G.: OpenRainER dataset, https://zenodo.org/records/10610886, accessed: 2025-02-20, 2024.

Crane, R. K.: Electromagnetic Wave Propagation through Rain, Wiley, New York, 1996.

Fencl, M., Nebuloni, R., Andersson, J. C., Bares, V., Blettner, N., Cazzaniga, G., Chwala, C., Colli, M., de Vos, L., El Hachem, A., et al.: Data formats and standards for opportunistic rainfall sensors, Open Research Europe, 3, 169, 2024.

Gelbart, L., Barthès, L., Mercier-Tigrine, F., Chazottes, A., and Mallet, C.: Enhanced quantitative precipitation estimation through the opportunistic use of Ku TV-SAT links via a dual-channel procedure, Atmospheric Measurement Techniques, 18, 351–370, 2025.

Giannetti, F., Reggiannini, R., Moretti, M., Adirosi, E., Baldini, L., Facheris, L., Antonini, A., Melani, S., Bacci, G., Petrolino, A., et al.: Real-time rain rate evaluation via satellite downlink signal attenuation measurement, Sensors, 17, 1864, 2017.

Giannetti, F., Moretti, M., Reggiannini, R., and Vaccaro, A.: The NEFOCAST system for detection and estimation of rainfall fields by the opportunistic use of broadcast satellite signals, IEEE Aerosp. Electron. Syst. Mag., 34, 16–27, 2019.

Gianoglio, C., Zani, S., Colli, M., and Caviglia, D. D.: Rainfall Classification in Genoa: Machine Learning vs. Adaptive Statistical Models Using Satellite Microwave Links, IEEE Access, 2024.

ITU-R P.838-3: Specific attenuation model for rain for use in prediction methods, Tech. rep., 2005.

https://doi.org/10.5194/essd-2025-537
Preprint. Discussion started: 4 December 2025

ITU-R P.839-4: Rain height model for prediction methods, Tech. rep., 2013.

Jacoby, D., Yu, S., Hu, S., Hine, Z., Johnson, R., Ostrometzky, J., Kadota, I., Messer, H., and Zussman, G.: OpenMesh dataset, zenodo,doi: 10.5281/zenodo.15268340., 2025.

Leijnse, H., Uijlenhoet, R., and Stricker, J. N. M.: Rainfall measurement using radio links from cellular communication networks, Water Resources Research, 43, https://doi.org/https://doi.org/10.1029/2006WR005631, 2007a.

Leijnse, H., Uijlenhoet, R., and Stricker, J. N. M.: Hydrometeorological application of a microwave link: 2. Precipitation, Water Resources Research, 43, 9, https://doi.org/https://doi.org/10.1029/2006WR004989, 2007b.

Mercier, F., Barthès, L., and Mallet, C.: Estimation of finescale rainfall fields using broadcast TV satellite links and a 4DVAR assimilation method, Journal of Atmospheric and Oceanic Technology, 32, 1709–1728, 2015.

Messer, H., Zinevich, A., and Alpert, P.: Environmental Monitoring by Wireless Communication Networks, Science, 312, 713–713, https://doi.org/10.1126/science.1120034, 2006.

Météo-France: Fiche climatologique, https://donneespubliques.meteofrance.fr/?fond=produit&id_produit=117&id_rubrique=39, accessed: 2025-05-13.

Nebuloni, R., Graf, M., Cazzaniga, G., Mercier, F., and Turko, M.: The OpenSat4Weather dataset: Ku-band satellite link data for precipitation monitoring, zenodo, doi: 10.5281/zenodo.16530166, 2025.

Overeem, A., Leijnse, H., and Uijlenhoet, R.: Two and a half years of country-wide rainfall maps using radio links from commercial cellular telecommunication networks, Water Resour. Res., 52, 8039–8065, https://doi.org/https://doi.org/10.1002/2016WR019412, 2016.

Tabary, P., Boumahmoud, A.-A., Andrieu, H., Thompson, R. J., Illingworth, A. J., Le Bouar, E., and Testud, J.: Evaluation of two "integrated" polarimetric Quantitative Precipitation Estimation (QPE) algorithms at C-band, Journal of Hydrology, 405, 248–260, 2011.

Thurai, M., Iguchi, T., Kozu, T., Eastment, J. D., Wilson, C. L., and Ong, J. T.: Radar observations in Singapore and their implications for the TRMM precipitation radar retrieval algorithms, Radio Science, 38, https://doi.org/https://doi.org/10.1029/2002RS002855, 2003.

Thurai, M., Deguchi, E., Okamoto, K., and Salonen, E.: Rain height variability in the Tropics, IEE Proceedings - Microwaves, Antennas and Propagation, 152, 17–23, https://doi.org/10.1049/ip-map:20041146, 2005.

Wilkinson, M. D., Dumontier, M., Aalbersberg, I. J., Appleton, G., Axton, M., Baak, A., Blomberg, N., Boiten, J.-W., da Silva Santos, L. B., Bourne, P. E., et al.: The FAIR Guiding Principles for scientific data management and stewardship, Scientific data, 3, 2016.